



Cite this: DOI: 10.1039/c7cp03439c

## Characterization of secondary phosphine oxide ligands on the surface of iridium nanoparticles†

 Israel Cano, <sup>\*a</sup> Luis M. Martínez-Prieto, <sup>a</sup> Pier F. Fazzini,<sup>a</sup> Yannick Coppel, <sup>bc</sup>  
Bruno Chaudret<sup>a</sup> and Piet W. N. M. van Leeuwen <sup>\*a</sup>

The synthesis of iridium nanoparticles (IrNPs) ligated by various secondary phosphine oxides (SPOs) is described. This highly reproducible and simple method *via* H<sub>2</sub> reduction produces well dispersed, small nanoparticles (NPs), which were characterized by the state-of-the-art techniques, such as TEM, HRTEM, WAXS and ATR FT-IR spectroscopy. In particular, multinuclear solid state MAS-NMR spectroscopy with and without cross polarization (CP) enabled us to investigate the different binding modes adopted by the ligand at the nanoparticle surface, suggesting the presence of three possible types of coordination: as a purely anionic ligand Ir–P(O)R<sub>2</sub>, as a neutral acid R<sub>2</sub>P–O–H and as a monoanionic bidentate H-bonded dimer R<sub>2</sub>P–O–H...O=PR<sub>2</sub>. Specifically, the higher basicity of the dicyclohexyl system leads to the formation of IrNPs in which the bidentate binding mode is most abundant. Such cyclohexyl groups are bent towards the edges, as is suggested by the study of <sup>13</sup>CO coordination on the NP surface. This study also showed that the number of surface sites on faces available for bridging CO molecules is higher than the number of sites for terminal CO species on edges and apices, which is unexpected taking into account the small size of the nanoparticles. In addition, the IrNPs present a high chemoselectivity in the hydrogenation of cinnamaldehyde to the unsaturated alcohol.

Received 22nd May 2017,  
Accepted 27th July 2017

DOI: 10.1039/c7cp03439c

rsc.li/pccp

## Introduction

The use of secondary phosphine oxides (SPOs) as stabilizing ligands for iridium nanoparticles (IrNPs) has been scarcely explored. Our group has a longstanding experience in the use of SPOs as multifunctional ligands, both in organometallic<sup>1–6</sup> and MNP<sup>6–10</sup> catalysis. SPOs may coordinate as a neutral acid (A),<sup>11,12</sup> a deprotonated phosphinito anion (B),<sup>13,14</sup> or a hydrogen bonded pair of the two (C),<sup>4–6,11</sup> thus obtaining a monoanionic, supramolecular bidentate ligand (Scheme 1).<sup>15</sup> In addition, the acid can be deprotonated to generate the O-metalated species D.<sup>16,17</sup>

We demonstrated the presence of P–O–H groups in ruthenium nanoparticles (RuNPs) ligated by SPOs through H<sub>2</sub>/D<sub>2</sub> isotope exchange reactions.<sup>7</sup> Along this line, our group developed the synthesis of gold nanoparticles (AuNPs) stabilized by SPO ligands.<sup>8,9</sup> An exhaustive characterization demonstrated that the nature of the ligand is a key feature, since important differences in the size, morphology and catalytic behavior were found to

depend on the hydrocarbyl substituents at phosphorus. Aromatic SPOs ligated to AuNPs present a strong polarity in their P=O bonds and they coordinate to the surface in their anionic form, B. In contrast, the more basic aliphatic phosphine oxides hold on more strongly to the protons and the actual coordination mode is at least in part the neutral acid A or the H-bonded dimer C. The AuNPs prepared with aryl-substituted SPOs were active catalysts for the highly chemoselective hydrogenation of substituted aldehydes. On the contrary, AuNPs containing alkyl SPOs showed low activity and selectivity. In a subsequent publication we described the formation of IrNPs stabilized with chiral SPOs,<sup>10</sup> in which we suggested a binding mode of the ligand on the IrNPs surface similar to that previously described for AuNPs ligated by aryl SPOs, *i.e.* a purely anionic SPO would be present. However, definite proofs were not obtained. These IrNPs were active catalysts for the asymmetric hydrogenation of ketones. Furthermore, we recently reported a comparative catalytic study in which a specific SPO ligand (*tert*-butyl-(phenyl)phosphine oxide) was employed to generate an Ir–SPO complex and SPO-stabilized IrNPs.<sup>6</sup> These Ir–SPO based catalysts showed markedly different selectivities and rates in the hydrogenation of various substituted aldehydes. This ligand coordinates as the H-bonded dimer C in the Ir–SPO complex, but the actual coordination mode of the SPO on the IrNP surface was not established.

Therefore, studies focusing on the location and possible types of coordination by the ligands present at the nanoparticle

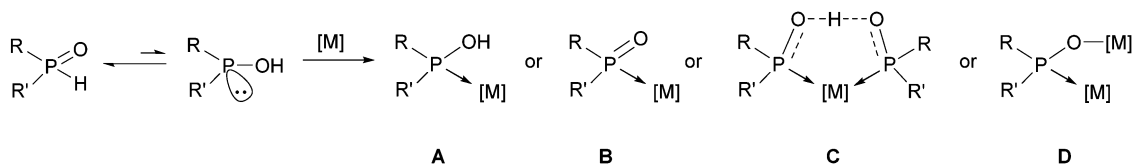
<sup>a</sup> Laboratoire de Physique et Chimie des Nano Objets, LPCNO, UMR5215 INSA-UPS-CNRS, Institut National des Sciences Appliquées, 135 Avenue de Rangueil, Toulouse 31077, France.

E-mail: israel.canorico@nottingham.ac.uk, vanleeuw@insa-toulouse.fr

<sup>b</sup> CNRS, LCC (Laboratoire de Chimie de Coordination) 205 Route de Narbonne, BP44099, F-31077 Toulouse Cedex 04, France

<sup>c</sup> Université de Toulouse, UPS, INPT, F-31077 Toulouse Cedex 04, France

† Electronic supplementary information (ESI) available. See DOI: 10.1039/c7cp03439c



Scheme 1 Tautomeric forms of SPOs and possible coordination modes to a metal center.

surface are of great importance, but the determination of the real binding mode remains difficult. Thus, inspired by these works, herein we report Magic Angle Spinning NMR (MAS-NMR) spectroscopy as a powerful tool that can provide insight in the morphology and coordination mode of SPO ligands at the surface and hence about the reactivity of the nanoparticles. To this end, a group of SPOs with different electronic and steric properties was selected for the generation of a series of IrNPs (Fig. 1).

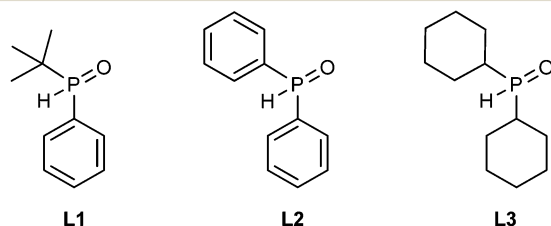


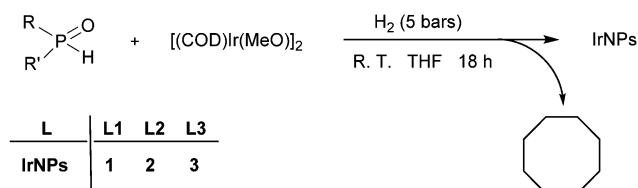
Fig. 1 Secondary phosphine oxides employed in this study.

The IrNPs were characterized by the use of a wide range of techniques, including Transmission Electron Microscopy (TEM), High Resolution TEM (HRTEM), Wide Angle X-Ray Scattering (WAXS) and Attenuated Total Reflectance Fourier-Transform Infrared (ATR FT-IR) spectroscopy. Specifically, MAS-NMR spectroscopy enabled us to explore the possible coordination modes adopted by the SPO ligand at the NP surface. Multinuclear solid state NMR techniques have been used to characterize the structure of ligands on MNPs and their surface chemistry as summarized in several recent reviews.<sup>18–21</sup>

## Results and discussion

### Synthesis and characterization of SPO-stabilized Ir nanoparticles

We chose the same protocol that was previously used for the synthesis of SPO-stabilized IrNPs.<sup>6,10</sup> The IrNPs 1–3 were prepared by H<sub>2</sub> reduction of (1,5-cyclooctadiene)(methoxy)iridium(i) dimer ([Ir(OMe)(COD)]<sub>2</sub>) in the presence of 0.5 eq. (based on Ir) of SPO L (Scheme 2, for further details see Section 2, ESI<sup>†</sup>).



Scheme 2 Synthesis of IrNPs 1–3 from [Ir(OMe)(COD)]<sub>2</sub> and L1–L3.

TEM micrographs revealed the presence of well distributed and small NPs (Fig. 2 and Section 6, ESI<sup>†</sup>) with a size in the range 1.3–1.5 nm (1, 1.33(0.28) nm; 2, 1.43(0.38) nm; 3, 1.39(0.50) nm), although 3 displayed a broader dispersion than 1 and 2 and some aggregation of NPs.

HRTEM images showed crystalline IrNPs compatible with a cubic close-packed structure (ccp). This was confirmed by Fast Fourier Transformation (FFT) analysis carried out on the HRTEM images as shown in Fig. S18 (ESI<sup>†</sup>). WAXS analysis confirmed the ccp structure and indicated a coherence length close to *ca.* 1.5 nm (Section 4, ESI<sup>†</sup>). These data are in agreement with the sizes determined by TEM and corroborate the crystallinity of the IrNPs.

Elemental analyses (EA) gave an Ir content in the range 48–50% and were consistent with a metal–ligand ratio of 1.85 : 1 for 1, 1.66 : 1 for 2, and 1.67 : 1 for 3 (Table 1). It is worth noting that the Ir/L ratio accounts for a large amount of SPO coordinated to the surface of the NP, since the approximate number of ligands is only slightly lower than the calculated number of surface atoms (estimated from IrNP mean size as observed by TEM).<sup>22</sup>

Table 1 Analytical data of IrNPs 1–3

IrNP	Diameter (nm)	Ir content (%)	Ir/L ratio	Ir <sub>x</sub> /L <sub>y</sub> <sup>a</sup>	N <sub>s</sub> <sup>b</sup>
1	1.33 ± 0.28	47.9	1.85 : 1	117/63	78
2	1.43 ± 0.38	50.4	1.66 : 1	145/87	91
3	1.39 ± 0.50	48.6	1.67 : 1	133/80	89

<sup>a</sup> The approximate composition is based on the Ir/L ratio and the number-average diameter measured. <sup>b</sup> Number of surface atoms. Approximate values obtained from the graphs of Van Hardeveld and Hartog.<sup>23</sup>

The ATR FT-IR spectra of free SPO ligands showed the P–H stretching absorption in the range 2280–2370 cm<sup>-1</sup> (Fig. S3, S5 and S8, ESI<sup>†</sup>). This P–H band was not visible in the ATR FT-IR spectra of 1–3 (Fig. S4, S6 and S9, ESI<sup>†</sup>), suggesting coordination of the ligand to the NP surface through the phosphorus atom. Additionally, no absorption was observed in the region corresponding to the (P–O)–H stretching band (*ca.* 3100–3500 cm<sup>-1</sup>). This lack of protons suggests that the phosphine adopts a coordination mode similar to that previously described for aryl SPO-ligated AuNPs (B).<sup>8,9</sup> However, this hypothesis could not be confirmed by ATR FT-IR spectroscopy, since the O–H–O vibration of the third possible coordination mode of SPO ligands to metals, that is as a monoanionic bidentate ligand with an intramolecular hydrogen bond (C), is usually not observed in IR.<sup>24</sup>

Finally, an intense band at *ca.* 1980–2005 cm<sup>-1</sup> was found in the spectra of IrNPs and recognized as CO coordinated to the

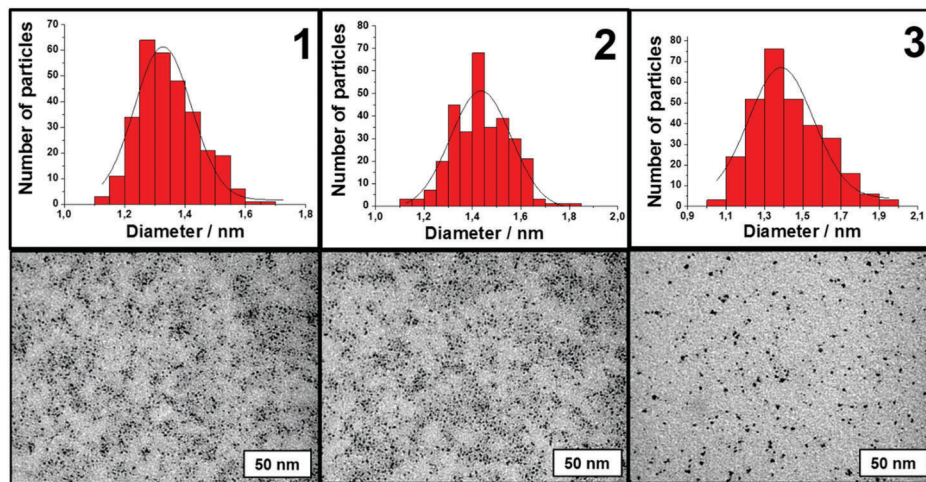


Fig. 2 Representative TEM micrographs of IrNPs **1–3** and size distributions determined from TEM images by counting >300 non-touching particles obtained from images captured from distinct quadrants of the grid.

NP surface, which probably results from a decarbonylation process of THF and/or methoxide during the NP formation.<sup>10,25</sup> The intensity of this band increased after bubbling CO through solutions of **1–3** in THF (R.T., 5 min, Fig. 3 and Section 5, ESI<sup>†</sup>), confirming the presence of coordinated CO at the Ir surface in the purified NPs. This band is identified as CO coordinated in a terminal mode (CO<sub>t</sub>), while another stretching band appears at lower frequency shift (*ca.* 1800 cm<sup>-1</sup>), which is assigned to CO coordinated in a bridging mode (CO<sub>b</sub>).<sup>26,27</sup> The ATR FT-IR spectra of **1–3** before bubbling with CO display a slight displacement in the CO<sub>t</sub> band to lower frequency following an increase in the electron-donor character of the substituents in the ligand, and thus in the presence of a more electron-rich iridium surface (Fig. S11, ESI<sup>†</sup>).<sup>28,29</sup> Conversely, an increase in the amount of CO on the NP surface involves a shift of the CO<sub>t</sub> stretching absorption to higher frequency (Fig. 3), as was earlier reported for metal surfaces.<sup>30–33</sup>

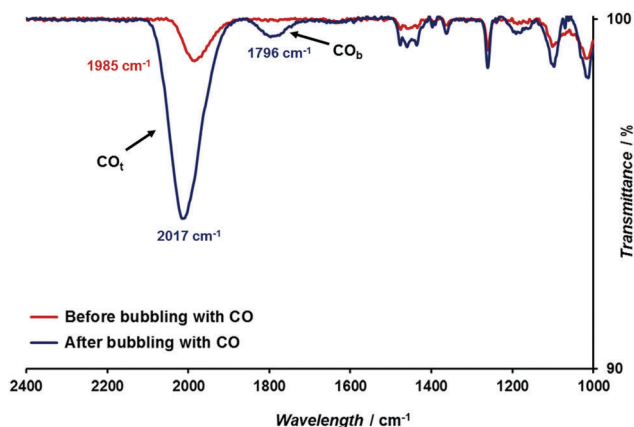


Fig. 3 Overlay of ATR-IR spectra of **1** before and after bubbling with CO in the region 1000–2400 cm<sup>-1</sup>. In view of the short contact times the spectra do not represent equilibrium states.

### Solid state NMR studies

Given the relatively limited information about the coordination modes of the ligands on the nanoparticle surface that can be obtained by FT-IR, we found solid state NMR to be a useful spectroscopic tool for this purpose. The coordination of ligands to the nanoparticle surface was demonstrated by solid state MAS NMR spectroscopy. <sup>31</sup>P MAS NMR spectra of IrNPs **1–3** (Fig. S19–S22, ESI<sup>†</sup>) showed broad heterogeneous signals centered around 68 ppm for **1**, 29 ppm for **2** and 94 ppm for **3**, with spectral range between 80 and 120 ppm. These broad signals are clearly different from the sharp ones of the corresponding free ligands (polymorphic crystal form signals centered at 42 ppm for **L1**, 17 ppm for **L2**, and 48 ppm for **L3**) with on average a resonance shift to higher frequency. The high frequency shift can be associated to the coordination of the ligand to the metal through the phosphorus atom, as is observed for molecular Ir–SPO complexes.<sup>6,11,14,34</sup> The spinning frequency for <sup>31</sup>P NMR experiments was set to 16 kHz (or above) to average the chemical anisotropy and the <sup>31</sup>P homonuclear dipolar couplings to zero. With this fast MAS NMR, the broadness and heterogeneity of <sup>31</sup>P signals corresponding to the ligands coordinated on the IrNP surface can be mostly associated to chemical and structural heterogeneities (or disorder).

Broadening contributions coming from magnetic field inhomogeneity, magnetic susceptibility and chemical shift distribution can be removed with a Carr–Purcell–Meiboom–Gill (CPMG) NMR experiment.<sup>35–44</sup> The <sup>31</sup>P resonances of IrNPs **1–3** showed strong sharpening in a CPMG experiment, confirming the presence of structural and chemical heterogeneities for SPO ligands at the IrNP surface (Fig. S23, ESI<sup>†</sup>). <sup>1</sup>H/<sup>31</sup>P HETCOR experiments with short contact time (0.3 ms) associated with CPMG detection to improve sensitivity showed that the different <sup>31</sup>P resonances of IrNPs **1–3** are not spatially close to the same hydrogen atoms (Fig. 4 and Fig. S24, S25, ESI<sup>†</sup>). In addition to the correlations with protons of organic substituents

(phenyl with  $\delta_{\text{H}} \sim 7.3$  ppm, cyclohexyl with  $\delta_{\text{H}} \sim 1.4$  ppm and *tert*-butyl with  $\delta_{\text{H}} \sim 1.2$  ppm groups), the  $^{31}\text{P}$  resonances showed dipolar correlations with  $^1\text{H}$  in the range between 6 and 14 ppm, indicating the presence of different OH groups close to  $^{31}\text{P}$  atoms, engaged in weak or strong hydrogen bonds. This proves that, in addition to the deprotonated anionic form **B**, monoanionic H-bonded dimer **C** (correlations with OH signal above 7 ppm) and neutral acid **A** (correlations with OH signal in the range 3–6 ppm) ligands are also present. For IrNPs **1** and **2** (Fig. S24 and S25, ESI $^\dagger$ ), the monoanionic bidentate coordination mode showed on average lower frequency shifts (heterogeneous signals centered around 42 ppm for **1** and 20 ppm for **2**, respectively) than the purely anionic form (heterogeneous signals centered around 80 ppm for **1** and 50 ppm for **2**, respectively), a trend generally observed for  $^{31}\text{P}$  resonances. Furthermore, the concentration of neutral acid species seems very low. For IrNPs **3** (Fig. 4), the heterogeneous signals centered around 94 ppm correspond mainly to H-bonded dimer species, while the neutral acid binding mode (dipolar correlations at  $\delta_{\text{P}} \sim 50$  ppm and  $\delta_{\text{H}} \sim 6.1$  ppm) is observed in a small ratio and anionic ligands seem to be a minority as is to be expected for the most basic ligand. The  $^1\text{H}/^{31}\text{P}$  CPMG-HETCOR experiment clearly illustrated the structural and chemical heterogeneity of the IrNPs samples.

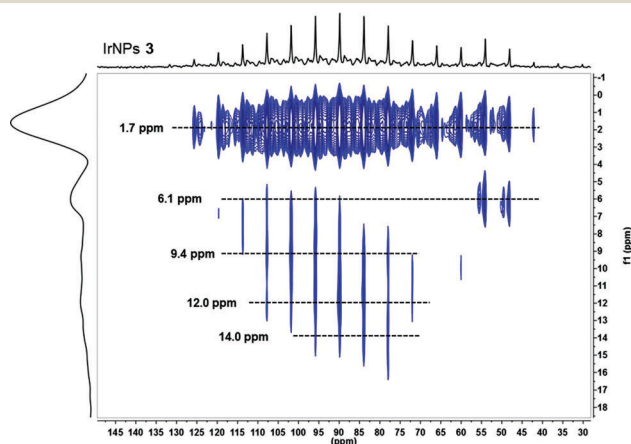


Fig. 4  $^{31}\text{P}$  CPMG-HETCOR MAS NMR spectrum of IrNPs **3**. Lines are given as guide to the eyes.

A broad  $^{31}\text{P}$  signal at higher frequency (centered around  $130(\pm 20)$  ppm with half-height linewidth of  $35(\pm 5)$  kHz) was

sometimes observed. This  $^{31}\text{P}$  signal has an unusual chemical shift for purely anionic or monoanionic H-bonded dimer species, with a short  $T_1^{\text{P}}$  relaxation time of  $60(\pm 20)$  ms compared to the  $T_1^{\text{P}}$  of the main  $^{31}\text{P}$  signals of IrNPs **1–3** (average  $T_1^{\text{P}}$  of  $5.7(\pm 0.7)$  s,  $7.8(\pm 1.1)$  s and  $10.7(\pm 2.0)$  s, for **1**, **2** and **3**, respectively). Due to its short  $T_1^{\text{P}}$ , this resonance can be edited in a  $^{31}\text{P}$  experiment using a  $T_1^{\text{P}}$  filter (Fig. S26, ESI $^\dagger$ ). We assigned this signal to Knight-shifted  $^{31}\text{P}$  resonances of ligand coordinated to coalesced IrNPs.<sup>45–51</sup> In transition metals such as iridium, the  $^{31}\text{P}$  NMR resonances of surface-adsorbed molecules on large MNPs experience a large paramagnetic shift, a Knight-shift,<sup>52</sup> due to the mixing of molecular orbitals with metal conduction bands of electrons.<sup>45,46</sup> Indeed, we have previously proved that the presence of conduction electrons at the surface of MNPs is related to their size, leading to the Knight-shift found in large NPs.<sup>52,53</sup>

The  $^{13}\text{C}$  MAS NMR spectra of **1–3** exhibit the characteristic signals belonging to the respective ligands present.  $^{13}\text{C}$  resonance broadenings after the SPO coordination to the IrNP surface are significantly less than the ones observed for the  $^{31}\text{P}$  resonances (Fig. S27–S29, ESI $^\dagger$ ), confirming the binding of the SPO ligands to the IrNPs through the phosphorus atoms. In addition, the  $^{13}\text{C}$  MAS NMR spectrum of **2** (Fig. S28, ESI $^\dagger$ ) presents a signal at *ca.* 28 ppm that corresponds to cyclohexyl groups obtained by a partial hydrogenation of phenyl groups during the synthesis under  $\text{H}_2$ . The small peak at *ca.* 67 ppm observed for **1–3** is likely due to MeOH.<sup>10</sup>

$^{13}\text{CO}$  was employed as a probe molecule to investigate the surface chemistry and the location of the open sites of these particles by solid state  $^{13}\text{C}$  MAS-NMR. Thus, solid samples of **1–3** were exposed to 1 bar of  $^{13}\text{CO}$  at R.T. for 20 h.  $^{13}\text{C}$  MAS spectra of **1–3** display new signals above 150 ppm corresponding to CO coordinated to the nanoparticle surface (Fig. S30, ESI $^\dagger$ ).<sup>10,54–58</sup> Two set of signals were identified (Table 2): (i) a broad signal centered at  $210 \pm 10$  ppm with spectral range of  $115 \pm 15$  ppm that belongs to CO coordinated in a bridging mode ( $\text{CO}_\text{b}$ ); (ii) a narrow signal centered at  $171 \pm 3$  ppm with spectral range of  $35 \pm 5$  ppm assigned to CO coordinated in a terminal mode ( $\text{CO}_\text{t}$ ).<sup>10</sup> Quantification of CO species was then performed in a Hahn-echo experiment with long recovery time (100 s, Fig. S30, ESI $^\dagger$ ). For the three samples, bridging CO molecules were the most abundant species with a CO population of 83, 75 and 58 ( $\pm 4$ )% of total CO for IrNPs **1**, **2** and **3**, respectively. Previous investigations on CO coordination over ruthenium nanoparticles

Table 2  $^{13}\text{C}$  NMR data of CO species in IrNPs **1–3**

IrNPs	<b>1</b>		<b>2</b>		<b>3</b>	
	$\text{CO}_\text{b}$	$\text{CO}_\text{t}$	$\text{CO}_\text{b}$	$\text{CO}_\text{t}$	$\text{CO}_\text{b}$	$\text{CO}_\text{t}$
$\delta$ (ppm)	$222 \pm 3$	$173 \pm 1$	$208 \pm 3$	$170 \pm 1$	$200 \pm 3$	$169 \pm 1$
Linewidth (ppm)	$120 \pm 5$	$37 \pm 2$	$127 \pm 6$	$38 \pm 2$	$103 \pm 4$	$31 \pm 2$
Ratio <sup>a</sup> (%)	$83 \pm 2$	$17 \pm 2$	$75 \pm 2$	$25 \pm 2$	$58 \pm 2$	$42 \pm 2$
$T_1^{\text{C}}$ (s)	$1.7 \pm 0.5$	$21.7 \pm 2.9$	$1.4 \pm 0.2$	$29.5 \pm 2.1$	$29.3 \pm 7.4$	$32.3 \pm 2.8$
$T_{1\text{S}}^{\text{C}}$ (ms)	$2.5 \pm 0.3$	$2.2 \pm 0.3$	$2.8 \pm 0.3$	$2.4 \pm 0.6$	$2.4 \pm 0.6$	$1.0 \pm 0.3$
$T_{1\text{P}}^{\text{H}}$ (ms)	$13 \pm 2$	$14 \pm 2$	$11 \pm 2$	$13 \pm 2$	$6 \pm 2$	$7 \pm 2$

<sup>a</sup> Ratio of bridging CO to terminal CO obtained by deconvolution of the Hahn-echo spectra (Fig. S31, ESI).

proved that CO<sub>b</sub> molecules coordinate onto faces and CO<sub>t</sub> onto edges and apices.<sup>25,59,60</sup> The higher relative amount of CO<sub>b</sub> molecules indicates that the number of surface sites available for these on faces is large in comparison with the corresponding sites for CO<sub>t</sub> on edges and apices, which is unexpected due to the small size of the IrNPs. Interestingly, the relative population of CO<sub>b</sub> is the smallest for 3 (58 ± 2% vs. 83 ± 2 and 75 ± 2% for 1 and 2), which points to a steric effect of cyclohexyl groups that restricts CO coordination on faces.

$T_1$  can be affected by motion on a time-scale of the Larmor frequency (in the ps to  $\mu$ s range).<sup>61</sup> The  $T_1^C$  of the two types of CO resonances were found very different for IrNPs 1 and 2 with respective values of  $1.7 \pm 0.5$  s,  $1.4 \pm 0.2$  s for CO<sub>b</sub> and  $21.7 \pm 2.9$  s,  $29.5 \pm 2.1$  s for CO<sub>t</sub> species. For IrNPs 3, the  $T_1^C$  of CO<sub>b</sub> and CO<sub>t</sub> species were more similar, with respective values of  $29.3 \pm 7.4$  and  $32.3 \pm 2.8$  s. The variations in  $T_1^C$  observed for CO<sub>b</sub> and CO<sub>t</sub> of 1 and 2 suggest a notable difference of local mobility for these species at the surface of IrNPs. The most likely explanation is a faster diffusion of the CO<sub>b</sub> molecules.<sup>62,63</sup> For IrNPs 3, the steric effect of the cyclohexyl groups and/or the presence of mainly monoanionic bidentate ligands could limit the CO<sub>b</sub> diffusion.

To get more information about the CO species, we studied their CP kinetics with <sup>1</sup>H (Fig. 5 and Fig. S32, ESI†). The CP kinetics should follow the classical I-S model,<sup>61</sup> since the H-CO heteronuclear dipolar interactions are expected to be weak (spatial remoteness) while the H-H homonuclear dipolar interactions should be moderate or strong. The CP kinetics in the I-S model is described by eqn (1):<sup>61</sup>

$$I = I(0)(1 - T_{1S}/T_{1p}^H)^{-1}[\exp(-t/T_{1p}^H)] - \exp(-t/T_{1S}) \quad (1)$$

in which  $t$  is the contact time,  $I(0)$  is the signal amplitude,  $T_{1S}$  is the CP time constant and  $T_{1p}^H$  is the proton spin-lattice relaxation time in the rotating frame. For IrNPs 1–3 the  $T_{1S}$  of CO<sub>t</sub> and CO<sub>b</sub> show differences (Table 2). For IrNPs 1 and 2 the  $T_{1S}$  difference between the two CO species is small ( $2.2 \pm 0.3$  ms vs.  $2.5 \pm 0.3$  ms and  $2.4 \pm 0.6$  ms vs.  $2.8 \pm 0.3$  ms for 1 and 2, respectively). However, for 3 the  $T_{1S}$  difference is more pronounced ( $1.0 \pm 0.3$  ms vs.  $2.4 \pm 0.6$  ms). The short  $T_{1S}$  observed for CO<sub>t</sub> of 3 can be explained by the high density of protons close to the terminal CO due to presence of the cyclohexyl groups, since  $T_{1S}$  is governed by internuclear distances ( $1/r^3$  factor) and the number of neighbouring protons. This is not surprising,

given that in a densely packed situation the O atoms of SPO ligands look at the faces, whereas the cyclohexyl substituents point to the edges and thus are closer to CO<sub>t</sub> molecules. The proton density and internal dynamics also affect the  $T_{1p}^H$ , which is the shortest for 3 ( $6.5 \pm 2$  ms) while it is longer for 1 and 2 ( $13.5 \pm 2$  and  $12.0 \pm 2$  ms, respectively). Note that the similar  $T_{1p}^H$  values observed for CO<sub>t</sub> and CO<sub>b</sub> were expected. Indeed, in a dense proton network, spin diffusion phenomena usually average the  $T_{1p}^H$  over few nm distances.

The collected NMR data demonstrated that IrNPs 1–3 are similar, but IrNPs 3 showed slight differences due to the presence of two cyclohexyl substituents in the ligand L3. The higher basicity or electron-donor character of the dicyclohexyl system (compared to diphenyl and *tert*-butyl(phenyl)) favors the coordination of the SPO ligand as the H-bonded dimer C, as was previously observed for AuNPs ligated by alkyl SPOs.<sup>9</sup> Their bulkiness also decreases the ratio of CO coordinated in a bridging mode to CO coordinated in a terminal mode and limits the mobility of CO<sub>b</sub> molecules.

### Catalytic hydrogenation of substituted aldehydes with 1–3

SPOs are an interesting alternative to common tertiary phosphorus ligands in catalysis because of their singular properties. Indeed, their corresponding metal complexes exhibit a particular ability to cleave H<sub>2</sub> heterolytically through the metal and the oxygen atom.<sup>1–6</sup> Our group applied this concept for hydrogenation reactions with Ru,<sup>7</sup> Au<sup>8,9,64</sup> and Ir<sup>6,10</sup> NPs stabilized by SPOs, for which the ligand plays a triple role, as stabilizer for nanoparticles, as modifying ligand, and as functional ligand supplying the oxygen function that participates in the heterolytic cleavage of dihydrogen. Along this line, we decided to evaluate the catalytic activity of IrNPs 1–3 in the chemoselective hydrogenation of cinnamaldehyde and *p*-nitrobenzaldehyde (Table 3). The optimal reaction conditions were found to be THF as the solvent, R.T. and 18 h as reaction time. The IrNPs were very selective to the carbonyl functionality in cinnamaldehyde and the corresponding cinnamyl alcohol was obtained with high chemoselectivity (entries 1–3). As shown, the smallest NPs, 1, are the most active ones, followed by 2 and 3. The former ones are the largest NPs and for the latter aggregation was observed which could lead to a decrease in activity. On the other hand, we observed a loss of selectivity in the hydrogenation of *p*-nitrobenzaldehyde (entries 4–6) and both aldehyde and nitro groups were

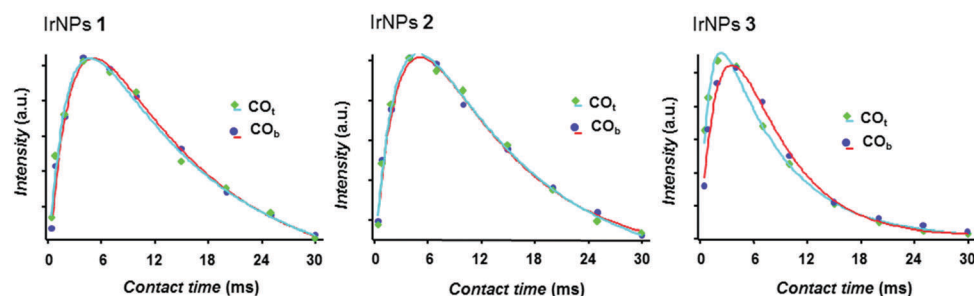
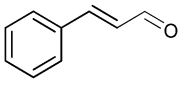
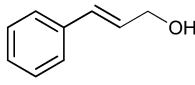
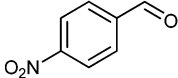
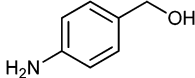


Fig. 5 <sup>13</sup>C CP/MAS kinetic curves for IrNPs 1–3.

Table 3 Catalytic hydrogenation of aldehydes with 1–3<sup>a</sup>

Entry	Substrate	IrNP	Product	Conversion <sup>b</sup> (%)	Selectivity <sup>c</sup> (%)
1		1		99	99 : 1 (UA : A)
2		72		98 : 2 (UA : A)	
3		61		98 : 2 (UA : A)	
4		1		> 99	95
5		2		> 99	50 <sup>d</sup>
6		3		> 99	95

<sup>a</sup> Reagents and conditions: 1–3 (0.0025 mmol Ir assuming % of Ir from elemental analysis), substrate (1 mmol), THF (0.75 mL), 18 hours, 293 K, 10 (entries 1–3) or 20 (entries 4–6) bar H<sub>2</sub>. <sup>b</sup> Conversions and product identities were determined by <sup>1</sup>H NMR spectroscopy (average of two runs).

<sup>c</sup> UA = unsaturated alcohol, A = saturated alcohol. <sup>d</sup> 4-Aminobenzaldehyde, azoarenes and other hydrogenation compounds as by-products.<sup>66,73</sup>

hydrogenated, affording 4-aminobenzyl alcohol as main product and other by-products resulting from nitro group hydrogenation, such as azoarenes and 4-aminobenzaldehyde. The reduction of nitroarenes to anilines has been extensively described with the use of MNPs.<sup>65–72</sup>

The IrNPs described herein do not exhibit any ligand effect and, except for slight variations, 1–3 display a similar catalytic behaviour. This is unsurprising since the ionic form **B** is not the exclusive binding mode of the SPOs for the IrNPs, and also the neutral acid **A** and the H-bonded dimer **C** exist at the nanoparticle surface. As a consequence, the Ir surface contains different active sites, which leads to a reduction in selectivity, in a similar way to the previously reported alkyl SPO AuNPs.<sup>9</sup> In this context, AuNPs ligated by SPOs showed drastic differences in the properties depending on the substituents in the ligand.<sup>8,9</sup> SPOs with aromatic substituents present R<sub>2</sub>P=O anions as the single type of ligand coordination, and thus electron-withdrawing SPOs could possibly do this for IrNPs.

## Conclusions

In summary, we have successfully used a series of secondary phosphine oxide ligands for the synthesis of iridium nanoparticles. The IrNPs showed a high chemoselectivity in the hydrogenation of cinnamaldehyde, although we observed a loss of selectivity for *p*-nitrobenzaldehyde and both aldehyde and nitro groups were hydrogenated. An extensive characterization of these nanoparticles was performed by several procedures. Specifically, we have proven that multinuclear solid state NMR spectroscopy is a powerful tool for the characterization of phosphine oxides directly attached to the IrNP surface, revealing structural and chemical heterogeneity of ligands at the surface. This study showed that the SPOs are bound to the NP surface by three coordination modes: as a purely anionic ligand Ir–P(O)R<sub>2</sub>, as the neutral acid R<sub>2</sub>P–O–H and as a monoanionic bidentate H-bonded dimer R<sub>2</sub>P–O–H ··· O=PR<sub>2</sub>. Interestingly, the bidentate binding mode is the most favored for **3** due to the higher basicity of the dicyclohexyl system.

In addition, the surface state of the nanoparticles was studied by <sup>13</sup>CO coordination. Solid state <sup>13</sup>C MAS-NMR experiments showed that the number of open sites on faces available for CO<sub>b</sub> is higher than the number of sites for CO<sub>t</sub> on edges and

apices, which is unexpected in view of the small size of the IrNPs. The IrNPs **3** exhibit the lowest relative population of CO<sub>b</sub> molecules, since the bulkiness of cyclohexyl groups and the presence of mainly monoanionic bidentate SPOs decrease the ratio of CO<sub>b</sub> to CO<sub>t</sub> and limits the mobility of both species.

In conclusion, thanks to solid state NMR we have elucidated the coordination modes adopted by SPO ligands at the NP surface, obtaining a clear picture of the surface of SPO-stabilized IrNPs. Therefore, multinuclear solid state NMR spectroscopy has shown its merit as a powerful technique for the comprehensive characterization of MNPs, which can aid the design of ligands that provide better catalytic properties.

## Conflicts of interest

There are no conflicts of interest to declare.

## Acknowledgements

We thank UPS-Toulouse and INSA for financial support. The authors acknowledge Dr Pierre Lacante for WAXS analyses (CEMES-CNRS). Prof. P. W. N. M. van Leeuwen thanks the Université Fédérale Toulouse Midi-Pyrénées for an IDEX Chaire d'Attractivité.

## Notes and references

- 1 P. W. N. M. van Leeuwen and C. F. Roobeek, *Eur. Pat. Appl.* EP 82576, 1983 (*Chem. Abstr.*, 1983, **99**, 121813).
- 2 P. W. N. M. van Leeuwen, C. F. Roobeek, R. L. Wife and J. H. G. Frijns, *J. Chem. Soc., Chem. Commun.*, 1986, 31–33.
- 3 P. W. N. M. van Leeuwen, C. F. Roobeek, J. H. G. Frijns and A. G. Orpen, *Organometallics*, 1990, **9**, 1211–1222.
- 4 P. W. N. M. van Leeuwen and C. F. Roobeek, *New J. Chem.*, 1990, **14**, 487–493.
- 5 P. M. Castro, H. Gulyas, J. Benet-Buchholz, C. Bo, Z. Freixa and P. W. N. M. van Leeuwen, *Catal. Sci. Technol.*, 2011, **1**, 401–407.
- 6 I. Cano, L. M. Martínez-Prieto, B. Chaudret and P. W. N. M. van Leeuwen, *Chem. – Eur. J.*, 2017, **23**, 1444–1450.

- 7 E. Rafter, T. Gutmann, F. Low, G. Buntkowsky, K. Philippot, B. Chaudret and P. W. N. M. van Leeuwen, *Catal. Sci. Technol.*, 2013, **3**, 595–599.
- 8 I. Cano, A. M. Chapman, A. Urakawa and P. W. N. M. van Leeuwen, *J. Am. Chem. Soc.*, 2014, **136**, 2520–2528.
- 9 I. Cano, M. A. Huertos, A. M. Chapman, G. Buntkowsky, T. Gutmann, P. B. Groszewicz and P. W. N. M. van Leeuwen, *J. Am. Chem. Soc.*, 2015, **137**, 7718–7727.
- 10 I. Cano, M. J.-L. Tschan, L. M. Martínez-Prieto, K. Philippot, B. Chaudret and P. W. N. M. van Leeuwen, *Catal. Sci. Technol.*, 2016, **6**, 3758–3766.
- 11 D. Martin, D. Moraleda, T. Achard, L. Giordano and G. Buono, *Chem. – Eur. J.*, 2011, **17**, 12729–12740.
- 12 F. Schröder, C. Tugny, E. Salanouve, H. Clavier, L. Giordano, D. Moraleda, Y. Gimbert, V. Mouriès-Mansuy, J.-P. Goddard and L. Fensterbank, *Organometallics*, 2014, **33**, 4051–4056.
- 13 C. Scriban, D. K. Wicht, D. S. Glueck, L. N. Zakharov, J. A. Golen and A. L. Rheingold, *Organometallics*, 2006, **25**, 3370–3378.
- 14 M. Liniger, B. Gschwend, M. Neuburger, S. Schaffner and A. Pfaltz, *Organometallics*, 2010, **29**, 5953–5958.
- 15 P. Sutra and A. Igau, *Coord. Chem. Rev.*, 2016, **308**, 97–116.
- 16 D. E. Fogg, N. J. Taylor, A. Meyer and A. J. Carty, *Organometallics*, 1987, **6**, 2252–2254.
- 17 D. E. Fogg and A. J. Carty, *Polyhedron*, 1988, **7**, 2285–2295.
- 18 B. Zhang and B. Yan, *Anal. Bioanal. Chem.*, 2010, **396**, 973–982.
- 19 T. Gutmann, I. del Rosal, B. Chaudret, R. Poteau, H.-H. Limbach and G. Buntkowsky, *ChemPhysChem*, 2013, **14**, 3026–3033.
- 20 T. Gutmann, A. Grünberg, N. Rothermel, M. Werner, M. Srour, S. Abdulhussain, S. Tan, Y. Xu, H. Breitzke and G. Buntkowsky, *Solid State Nucl. Magn. Reson.*, 2013, **55–56**, 1–11.
- 21 L. E. Marbella and J. E. Millstone, *Chem. Mater.*, 2015, **27**, 2721–2739.
- 22 In addition, the presence of nanoparticles too small (<13 atoms) to be observed by the TEM equipment is likely, since very small spots were sometimes observed. This would explain the high ratio of SPO ligands.
- 23 R. Van Hardeveld and F. Hartog, *Surf. Sci.*, 1969, **15**, 189–230.
- 24 P. Mastrorilli, M. Latronico, C. F. Nobile, G. P. Suranna, F. P. Fanizzi, U. Englert and G. Ciccarella, *Dalton Trans.*, 2004, 1117–1119.
- 25 L. M. Martínez-Prieto, C. Urbaneja, P. Palma, J. Cámpora, K. Philippot and B. Chaudret, *Chem. Commun.*, 2015, **51**, 4647–4650.
- 26 J. S. Bradley, J. M. Millar, E. W. Hill, S. Behal, B. Chaudret and A. Duteil, *Faraday Discuss.*, 1991, **92**, 255–268.
- 27 A. Duteil, R. Quéau and B. Chaudret, *Chem. Mater.*, 1993, **5**, 341–347.
- 28 F. Dassenoy, K. Philippot, T. O. Ely, C. Amiens, P. Lecante, E. Snoeck, A. Mosset, M.-J. Casanove and B. Chaudret, *New J. Chem.*, 1998, 703–711.
- 29 E. Ramírez, L. Eradès, K. Philippot, P. Lecante and B. Chaudret, *Adv. Funct. Mater.*, 2007, **17**, 2219–2228.
- 30 R. P. Eischens and W. A. Pliskin, *Adv. Catal.*, 1958, **10**, 1–56.
- 31 A. M. Bradshaw and F. M. Hoffmann, *Surf. Sci.*, 1978, **72**, 513–535.
- 32 S. Kinayyigit, P. Lara, P. Lecante, K. Philippot and B. Chaudret, *Nanoscale*, 2014, **6**, 539–546.
- 33 L. M. Martínez-Prieto, I. Cano, A. Márquez, E. A. Baquero, S. Tricard, L. Cusynato, I. del Rosal, R. Poteau, Y. Coppel, K. Philippot, B. Chaudret, J. Campora and P. W. N. M. van Leeuwen, *Chem. Sci.*, 2017, **8**, 2931–2941.
- 34 J. A. S. Duncan, D. Hedden, D. M. Roundhill, T. A. Stephenson and M. D. Walkinshaw, *Angew. Chem.*, 1982, **94**, 463–464.
- 35 J. T. Cheng and P. D. Ellis, *J. Phys. Chem.*, 1989, **93**, 2549–2555.
- 36 B. A. Cowans and J. B. Grutzner, *J. Magn. Reson., Ser. A*, 1993, **105**, 10–18.
- 37 F. H. Larsen, H. J. Jakobsen, P. D. Ellis and N. C. Nielsen, *J. Phys. Chem. A*, 1997, **101**, 8597–8606.
- 38 F. H. Larsen, H. J. Jakobsen, P. D. Ellis and N. C. Nielsen, *Mol. Phys.*, 1998, **95**, 1185–1195.
- 39 A. S. Lipton, J. A. Sears and P. D. Ellis, *J. Magn. Reson.*, 2001, **151**, 48–59.
- 40 The CPMG experiment has been used lately to improve NMR spectra of spin 1/2 of heterogeneous materials where distribution of frequencies, not refocused by MAS, can be refocused by rf pulses to compress the range of chemical shifts into spikelets and quicken signal acquisition. See ref. 41–44.
- 41 R. Siegel, T. T. Nakashima and R. E. Wasylshen, *J. Phys. Chem. B*, 2004, **108**, 2218–2226.
- 42 J. W. Wiench, V. S.-Y. Lin and M. Pruski, *J. Magn. Reson.*, 2008, **193**, 233–242.
- 43 M. Dechamps, C. Roiland, B. Bureau, G. Yang, L. Le Pollès and D. Massiot, *Solid state Nucl. Magn. Reson.*, 2011, **40**, 72–77.
- 44 K. J. Harris, Z. E. M. Reeve, D. Wang, X. Li, X. Sun and G. R. Goward, *Chem. Mater.*, 2015, **27**, 3299–3305.
- 45 W. D. Knight, *Phys. Rev.*, 1949, **76**, 1259–1260.
- 46 J. J. van der Klink and H. B. Brom, *Prog. Nucl. Magn. Reson. Spectrosc.*, 2000, **36**, 89–201.
- 47 S. E. Shore, J. P. Ansermet, C. P. Slichter and J. H. Sinfelt, *Phys. Rev. Lett.*, 1987, **58**, 953–956.
- 48 J. S. Bradley, J. M. Millar and E. W. Hill, *J. Am. Chem. Soc.*, 1991, **113**, 4016–4017.
- 49 L. R. Becerra, C. P. Slichter and J. H. Sinfelt, *J. Phys. Chem.*, 1993, **97**, 10–12.
- 50 L. R. Becerra, C. P. Slichter and J. H. Sinfelt, *Phys. Rev. B: Condens. Matter Mater. Phys.*, 1995, **52**, 11457–11461.
- 51 K. W. Zilm, L. Bonneviot, D. M. Hamilton, G. G. Webb and G. L. Haller, *J. Phys. Chem.*, 1990, **94**, 1463–1472.
- 52 J. M. Asensio, S. Tricard, Y. Coppel, R. Andrés, B. Chaudret and E. de Jesús, *Angew. Chem., Int. Ed.*, 2017, **56**, 865–869.
- 53 Small MNPs (<100 metal atoms) tend to behave as molecular species without free electrons and no Knight shift is observed. See e.g. J. S. Bradley, J. M. Millar, E. W. Hill and S. Behal, *J. Catal.*, 1991, **129**, 530–539.
- 54 See ref. 55–58 for a variety of examples related to coordination of CO at iridium complexes in a bridging and terminal mode.
- 55 B. E. Mann, B. T. Pickup and A. K. Smith, *J. Chem. Soc., Dalton Trans.*, 1989, 889–893.

- 56 S. Moreton, *Inorg. Chim. Acta*, 1992, **202**, 225–230.
- 57 L. Garlaschelli, F. Greco, G. Peli, M. Manassero, M. Sansoni, R. Gobetto, L. Salassa and R. D. Pergola, *Eur. J. Inorg. Chem.*, 2003, 2108–2112.
- 58 A. Tassan, M. Mozzon, G. Facchin, A. Dolmella and S. Detti, *Inorg. Chim. Acta*, 2015, **424**, 91–102.
- 59 F. Novio, K. Philippot and B. Chaudret, *Catal. Lett.*, 2010, **140**, 1–7.
- 60 L. M. Martínez-Prieto, A. Ferry, P. Lara, C. Richter, K. Philippot, F. Glorius and B. Chaudret, *Chem. – Eur. J.*, 2015, **21**, 17495–17502.
- 61 W. Kolodziejewski and J. Klinowski, *Chem. Rev.*, 2002, **102**, 613–628.
- 62 P.-K. Wang, J.-P. Ansermet, C. P. Slichter and J. H. Sinfelt, *Phys. Rev. Lett.*, 1985, **55**, 2731–2734.
- 63 L. R. Becerra, C. A. Klug and C. P. Slichter, *J. Phys. Chem.*, 1993, **97**, 12014–12019.
- 64 N. Almora-Barrios, I. Cano, P. W. N. M. van Leeuwen and N. Lopez, *ACS Catal.*, 2017, **7**, 3949–3954.
- 65 See ref. 66–69 for a variety of reviews related to the reduction of nitroarenes catalyzed by MNPs and ref. 70–72 for several examples concerning the reduction of nitroarenes catalyzed by IrNPs.
- 66 H.-U. Blaser, H. Steiner and M. Studer, *ChemCatChem*, 2009, **1**, 210–221.
- 67 P. Lara and K. Philippot, *Catal. Sci. Technol.*, 2014, **4**, 2445–2465.
- 68 H. Chong and M. Zhu, *ChemCatChem*, 2015, **7**, 2296–2304.
- 69 T. Aditya, A. Pal and T. Pal, *Chem. Commun.*, 2015, **51**, 9410–9431.
- 70 G.-Y. Fan, L. Zhang, H.-Y. Fu, M.-L. Yuan, R.-X. Li, H. Chen and X.-J. Li, *Catal. Commun.*, 2010, **11**, 451–455.
- 71 C. Campos, C. Torres, M. Oportus, M. A. Peña, J. L. G. Fierro and P. Reyes, *Catal. Today*, 2013, **213**, 93–100.
- 72 A. B. Dongil, C. Rivera-Cárcamo, L. Pastor-Pérez, A. Sepúlveda-Escribano and P. Reyes, *Catal. Today*, 2015, **249**, 72–78.
- 73 L. Hu, X. Cao, L. Chen, J. Zheng, J. Lu, X. Sun and H. Gu, *Chem. Commun.*, 2012, **48**, 3445–3447.